This is an *Accepted Manuscript*, which has been through the Royal Society of Chemistry peer review process and has been accepted for publication.

Accepted Manuscripts are published online shortly after acceptance, before technical editing, formatting and proof reading. Using this free service, authors can make their results available to the community, in citable form, before we publish the edited article. We will replace this *Accepted Manuscript* with the edited and formatted *Advance Article* as soon as it is available.

You can find more information about *Accepted Manuscripts* in the **Information for Authors**.

Please note that technical editing may introduce minor changes to the text and/or graphics, which may alter content. The journal's standard **Terms & Conditions** and the **Ethical guidelines** still apply. In no event shall the Royal Society of Chemistry be held responsible for any errors or omissions in this *Accepted Manuscript* or any consequences arising from the use of any information it contains.

Wednesday, March 16, 2016

Title :

Non-symmetric benzo[b]-fused BODIPYs as a versatile fluorophore platform reaching the NIR: A systematic study of the underlying structure–property relationship†

*André Bessette[1,2], Thomas Auvray[1], Denis Désilets[2] and Garry S. Hanan[1] *.*

[1] Département de Chimie, Université de Montréal, Pavillon J.-A. Bombardier, 5155 Decelles Avenue, Montréal, Québec, H3T-2B1, Canada. E-mail: garry.hanan@umontreal.ca

[2] PCAS Canada Inc. (www.pcas.com), 725 Trotter street, Saint-Jean-sur-Richelieu, Québec, J3B 8J8, Canada. E-mail: denis.desilets@pcascanada.com

RECEIVED DATE (automatically inserted by publisher);

ABSTRACT

Ten newly synthesized non-symmetric benzo[*b*]-fused BODIPYs are compared with an extended series of nine related families (23 compounds) to gain insights into their structure–property relationship. The insertion of a fused indole moiety in the dipyrromethene core and variation of various substituents on the proximal aryl, including fused aromatic groups, lead to pronounced changes in the properties of compounds **1 – 10**. By taking advantage of this versatile synthetic platform that allows facile substituent modifications and extension of the π-conjugated system, significant bathochromic shifts in the absorption (λ_{max} = 511 – 597 nm) and emission (601 – 757 nm) bands are achieved. Although the oxidation potentials of the compounds varies considerably through the series (+1.28 – +1.65 V) due to the significant contribution of the aryl function to the HOMO, the reduction remains much more consistent (-0.61 to -0.79 V) as the LUMO resides primarily on the dipyrromethene core with little aryl contribution as calculated by DFT. For example, installation of a dimethylamine substituent in the para position of the aryl group leads to dramatic modification of the optoelectronic properties of the absorption (597 nm) and emission (757 nm) maxima. The full electrochemical, photophysical and computational analyses of the compounds and the structural characterization of compounds **1**, **5**, **8**, and **9** are further used to rationalize the potential of this powerful platform.

KEYWORDS

2

INTRODUCTION

BODIPYs have proved to be highly versatile fluorescent dyes owing to their remarkable photophysical properties including intense absorption in the red, bright fluorescence, photochemical and thermal stabilities along with inertness towards pH and fluctuations in polarity.[1, 2] The 4,4-difluoro-4-bora-3a,4a-diaza-*s*-indacene skeleton on which it is based has been the focus of intense research in the last decades in order to modulate the optoelectronic properties so as to extend its range of action towards the deep-red and near-infrared (NIR) (refer to Figure 1 for nomenclature).[3-5] Great benefits come with harnessing the lower energy part of the visible / NIR spectrum, such as more efficient photovoltaic materials and improved sensibility in biological applications where the body absorbs most of the high-energy visible photons.[6-9] BODIPYs were hence integrated in an abundance of useful applications such as fluorescence imaging,[8-12] cancer photodynamic therapy,[13-15] metal-free photocatalysis,[16-19] electrochemiluminescence,[20] OLEDs and laser dyes;[21] transistors,[22] artificial light-harvesting antenna,[23-25] hydrogen production,[26, 27] organic photovoltaic (OPV) and dye-sensitized solar cells (DSSC);[3, 28-31] all of which require the ability to fine-tune their properties. Multiple structural modifications at the periphery and at the boron atom were studied, thanks to the rich chemistry accessible on all the positions of the core.[1, 3, 5, 32] Besides, replacing the *meso* carbon atom on the skeleton by a nitrogen atom affords the closely related family of aza-BODIPYs with red-shifted optical properties. The BF_2 chelate itself can also be replaced to use the dipyrromethene (DPM) and aza-dipyrromethene (ADPM) cores as ligands for various metals.[3, 33-35] The design of non-symmetric derivatives is another efficient way to significantly alter the optoelectronic properties, notably by generating a push-pull effect that reduces the HOMO-LUMO gap (ΔE).[36-41] Recently, much attention was devoted to extending the π-conjugated system of BODIPYs through ring-fusing strategies, with a selection of relevant examples illustrated in Figure 1. Among them, the

benzannulation of one pyrrole at the [*b*] bound proved to be an interesting avenue to obtain a narrower ΔE as compared to the same type of fusing at the [*a*] bound. In fact, Wakamiya *et al.* showed that the non-symmetric benzo[*b*]-fused skeleton can be regarded as a combination of the electron-donating (EDG) pyrrole and the electron-withdrawing (EWG) azafulvene moieties that generates a push-pull effect within the BODIPY core.[42] The enhanced azafulvene character in this type of fused system decreases the LUMO while maintaining a moderate increase of the HOMO, a combination of effects that is highly suitable for the design of air-stable NIR dyes. In our ongoing efforts to harvest the NIR photons for energy conversion applications,[43-47] we were attracted by the obvious advantages of the benzo[*b*]-fused BODIPY (BbF) platform and made the hypothesis that combining the push-pull effect obtained through non-symmetry of the core with various electron-rich proximal aryl groups directly connected on the EDG pyrrole moiety would allow significant modulation of the optoelectronic properties. Non-symmetric BbF **1 – 10** were prepared based on a versatile synthetic methodology allowing easy substituent modifications and extension of the π-conjugated system (Scheme 1). A critical analysis was undertaken to ascertain the effect of the fusion mode within the BbF series and across an extensive series of 23 derivatives from 9 different BODIPY families (Figure 1). The structure-property relationship was established through electrochemistry, spectroscopy, computational modelization and the X-ray structural characterization of key BbF derivatives **1**, **5**, **8** and **9**.

Scheme 1 – Synthesis of non-symmetric benzo[b]-fused BODIPYs (BbF) **1** – **10**.

Yields over two steps; refer to ESI for specific conditions of BbF **8**. Fragmentation colour code for analysis: Blue = benzo[b]-fused DPM core, Green = meso-phenyl, Red = BF2 chelate, Black = proximal aryl substituent.
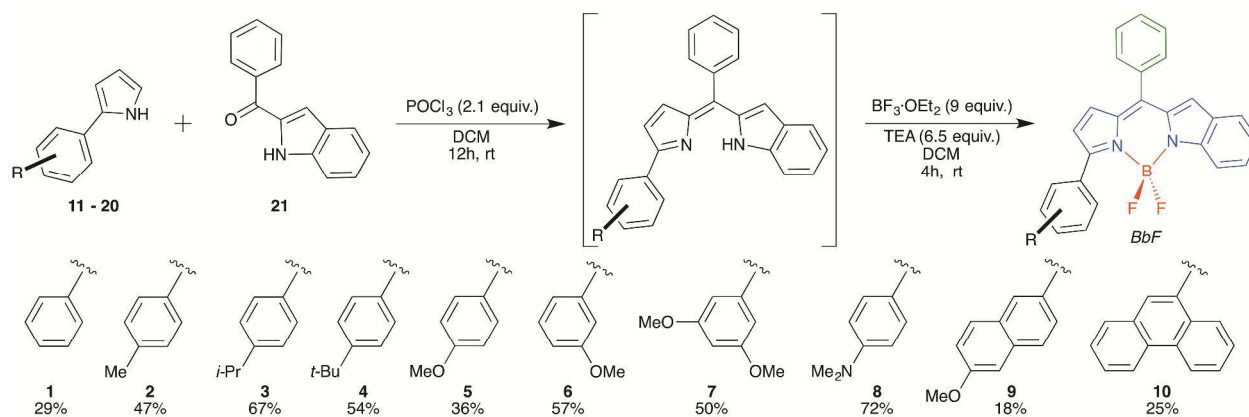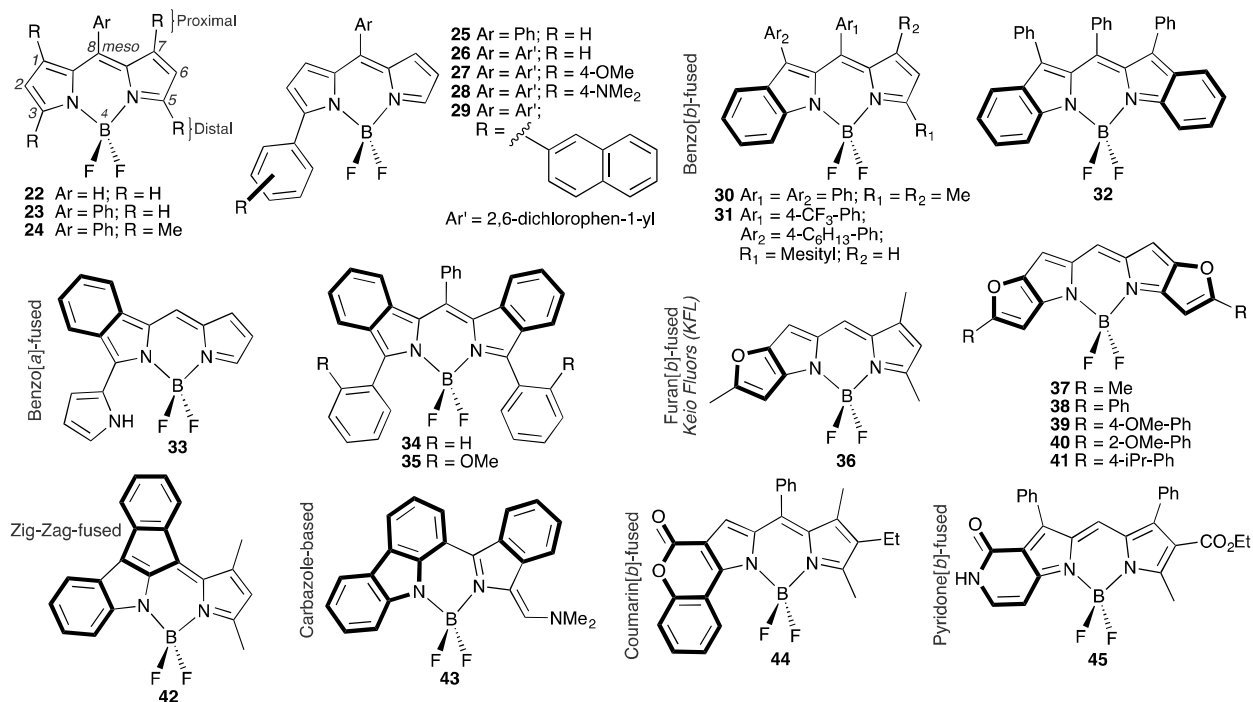
Figure 1 – Related BODIPYs of interest discussed herein. Refer to Table S.1 of ESI for a compilation of the optoelectronic properties previously reported in literature.†

RESULTS AND DISCUSSION

Taking advantage of a versatile synthetic platform

Inspired by two recent studies looking at the impact of the fusion mode in benzene-fused BODIPYs,[42, 48] we undertook to synthetize the series of ten non-symmetric benzo[*b*]-fused BODIPYs **1** – **10** where the proximal aryl substituent is systematically altered with electron-rich substituents (Scheme 1 and Synthetic Methods of ESI†). The main objective is to gain insights into the range of optoelectronic tuning achievable through proximal aryl substitution in order to reach the NIR spectral region and suitable energy levels in both photovoltaic and life sciences applications.[3, 5, 8, 49] Therefore, our two-steps synthetic methodology was based on the initial reaction of the corresponding aryl-pyrrole **11** – **20** with (1*H*-indol-2-yl)(phenyl)methanone **21** in presence of 2.1 equivalents of phosphoryl chloride in CH_2Cl_2 at room temperature. The benzo[*b*]-fused dipyrromethene intermediates thus formed were isolated as crude products, followed by the coordination of the BF_2 chelate upon reaction with a large excess of boron trifluoride diethyl etherate and triethylamine (TEA). The yields over two-steps obtained varied from a modest 18% in the case of 6-methoxynaphthalen-2-yl substituted BbF **9** up to 67% for BbF **3** bearing a *p-^{i}*Pr-phenyl. In the specific case of BbF **8**, it was observed that the first step of the methodology should also include 1.1 equivalent of TEA in order to keep the dimethylamine group deprotonated during the synthesis and was followed by air exposure to insure complete oxidation to the dipyrromethene intermediate (refer to ESI†). In this manner, the overall yield reached 72%. Crystals suitable for X-ray diffraction analysis were obtained for BbF derivatives **1**, **5**, **8** and **9**, which displayed extended conjugation throughout the benzo[*b*]-fused DPM core, partial conjugation with the proximal aryl substituents and almost no conjugation at all with the *meso* phenyl in the solid state (Figure 7 and corresponding X-ray section). Of note, both pyrrolic and indolic fragments on which the synthetic platform is based provide a rich chemistry where all the

positions, including the *meso-* one, can easily be modified either separately or all at once to fit specific application requirements.[3, 32, 50-54] Overall, this synthetic approach is tolerant to substitution of the proximal aryl with different alkyl chains (**1** – **4**), electron-donating groups in *para* (**5** and **8**) or electron-withdrawing groups in *meta* (**6** and **7**) along with implementation of extended π-conjugated systems (**9** and **10**).[55]

Electrochemical Properties

    Insights from electrochemistry are essential to establish if ground state energy levels and overall stability of BODIPYs **1** – **10** are suitable for use in the previously mentioned applications. For example, efficient electron transfer upon photoexcitation in OPV and DSSC require a proper match between the LUMO levels of both the donor (D) and acceptor (A).[6, 56] Equally, the HOMO level must imperatively lie below the air oxidation threshold in order to avoid accelerated degradation of fluorescent sensors and photovoltaic devices.[57, 58] The electrochemical properties of the benzo-[*b*]-fused BODIPY series **1** – **10** were investigated by differential-pulsed voltammetry (DPV) and cyclic voltammetry (CV) techniques in CH_2Cl_2 (Table 1 and ESI†; DPV redox potentials are given in the text unless otherwise noted) and were compared to previously reported electrochemical data found for some related derivatives (Figure 1 and Table S.1†). Combined with the computational modelization studies made by DFT (Table 2; Figures 2 and 4), these two techniques provide critical information regarding the HOMO / LUMO energy levels and the stability of electronic processes.

Table 1 – Electrochemical data for BbF **1 – 10**.

	E_{Ox} [a]	E_{Red} [a]
1	1.55, 1.45, 1.33	-0.67 (-0.68 [126])[b], -1.57, -1.78
2	1.65, 1.55, 1.36	-0.64 (-0.66 [163])[b], -1.54, -1.62
3	1.61, 1.52, 1.33	-0.68 (-0.67 [145])[b], -1.53, -1.60
4	1.48, 1.44, 1.27	-0.61 (-0.64 [150])[b], -1.49, -1.53
5	1.54, 1.46, 1.31	-0.64 (-0.70 [164])[b], -1.49, -1.52
6	1.54, 1.39, 1.28	-0.67 (-0.62 [160])[b], -1.58, -1.67
7	1.39	-0.65 (-0.61 [155])[b], -1.54, -1.58
8	1.68, 1.50, 1.40, 0.88	-0.79 (-0.78 [179])[b], -1.57, -1.64
9	1.50, 1.40, 1.26	-0.65 (-0.64 [109])[b], -1.51, -1.55
10	1.65, 1.58, 1.40	-0.64 (-0.64 [141])[b], -1.52, -1.58

[a] Determined by DPV. Potentials are in volts *vs*. SCE for CH_2Cl_2 deaerated solutions, 0.1 M of TBAP, recorded at 25 ± 1 °C at a sweep rate of 50 mV/s. Irreversible process unless otherwise stated. [b] Pseudo-reversible process. Half-wave potential determined by CV given in parentheses with the difference between cathodic and anodic peak potentials (mV) in brackets.

The electrochemical data in Table 1 and associated cyclic voltammograms presented in the ESI (Figures S.42 – S.61†) show that the BbF series present irreversible oxidation processes along with a first reversible reduction followed by two closely separated irreversible processes. In the case of reference adduct **1** bearing an unsubstituted proximal phenyl, three irreversible oxidations are found at 1.33, 1.45 and 1.55 V *vs*. SCE. DFT calculations suggest that the first oxidation is more likely to happen on the delocalized π-system including the benzo[*b*]-fused DPM core and the proximal phenyl, with almost no contribution from either the *meso*-phenyl or the BF$_2$ fragments (Figure 4). On the reduction side, the first reversible process at -0.67 V (see Table 2) is followed by two distinct irreversible processes at -1.57 and -1.78 V. The calculated LUMO, a first approximation of the most likely fragments to receive an electron, suggests that it involves mainly the DPM core and its *meso*-phenyl with a decreased contribution from the

8

proximal aryl group. These observations are in line with the calculations of Wakamiya *et al.* where the HOMO was associated with the electron-rich pyrrole fragment while the LUMO mainly involved the electron-poor indole with an increased azafulvene character.[42]

Interestingly, the fully unsubstituted BODIPY **22** presents only two irreversible processes, at 1.61 V for its oxidation and -0.73 V for its reduction, while the *meso*-phenyl substituted **23** irreversibly oxidizes at slightly higher potential (1.65 V) and has a first reversible reduction also at -0.73 V followed by an irreversible one at -1.71 V (Table S.1†).[59, 60] Thus, the *meso*-phenyl moiety found both in benzo[*b*]-fused BODIPY **1** and unfused derivative **23** contributes to the reversibility of the first reduction process, and an additional irreversible reduction each at -1.78 and -1.71 V, respectively. This finding is also in accordance with the DFT calculations (*vide supra*). On the other hand, the presence of blocking groups on the 1,3,5,7 positions of the BODIPY core, such as the methyl in adduct **24**, allow for a reversible first oxidation process (1.51 V).[48] The absence of such blocking groups on the distal side of the BbF **1** – **10** series, therefore, appears to be in part responsible for the irreversible first oxidation that is observed. Another important element to consider is how the replacement of the pyrrole by an indole moiety in fused systems affects the overall stability towards oxidation. The electrochemical data of closely related derivatives indicates that the [*b*]-fused indole moiety itself might give rise to the instability since fully capped derivatives **30** (non-symmetric; 1.57 V) and **32** (symmetric; 1.66 V) both have an irreversible first oxidation, just as uncapped derivative **31** (1.51 V) does.[42, 48] In contrast, fully substituted symmetric benzo[*a*]-fused **34** and **35** present reversible first oxidations at much less positive oxidation potentials (0.83 and 0.78V, respectively).[61] Of note, a fully-fused BODIPY, dimerized through the [*b*] bound based on the structure of **31**, was found to offer reversibility of the first oxidation process even though it was uncapped on the pyrrole fragments,[42] thus paving the way towards stable benzo[*b*]-fused system.

An interesting difference on the redox properties is observed upon substitution with various alkyl chains at the *para* position of the proximal aryl. With respect to reference BbF **1**, introduction of a methyl group in adduct **2** changes the first oxidation potentials by +30 mV (1.36V) and the second and third by +100 mV (1.55 and 1.65 V). All three reductions are easier to access by the same ~30 mV amount (-0.64, -1.54 and -1.62 V). Isopropyl substituted BbF **3** oxidizes at the same potential as compound **1** (1.33 V) and is complemented with stabilized second and third oxidation processes (1.52 and 1.61 V). Similarly, the first reduction is almost identical at -0.68 V to that of **1** with slightly less negative second and third processes (-1.53 and 1.60 V, respectively). In contrast, all three oxidation processes of ^{t}Bu derivative **4** are destabilized (1.27, 1.44 and 1.48 V) due to stronger electron donation, while the reduction ones are significantly less negative (-0.61, -1.49 and -1.53 V) relative to BbF **1**. The increase in the oxidation potentials within the BbF **2** – **4** series is not in full agreement with the Hammett parameter trend expected (Me: σ_p = -0.17; ^{i}Pr: σ_p = -0.15; ^{t}Bu: σ_p = -0.20),[62] as **3** displays a more difficult oxidation than **2**. However, the bulky and electron-rich ^{t}Bu derivative **4** is markedly affected as compared to the smaller alkyl groups of **2** and **3**. The reduction potentials of BbF **2** and **3** are similar to the reference **1**, pointing towards little influence of proximal aryl groups in the energy of the LUMO. There also exists a mismatch of the redox potentials of the BbF **2** – **4** series relative to **1** that might find its source in a poor electronic delocalization between the proximal phenyl and the benzo[*b*]-fused DPM core of the later compound. DFT calculations with PCM of CH_2Cl_2 support this assumption by the presence of two partial nodes on the *meta* carbons of the proximal phenyl in the HOMO of **1** and a higher dihedral angle between the two fragments (φ = 34.74° for **1** *vs.* 33.03° for **2**, 33.46° for **3** and 33.07° for **4**). Another important point to consider is that extended conjugation in BbF **2** – **4** causes a notable decrease and alteration of the dipole moments *vs.* **1** (refer to Figure 4) that hamper redox

processes due to reduced polarizability within the molecules. Thus, it appears the choice of alkyl chains on the proximal aryl isn't as innocent as one would *a priori* expect from an electrochemical perspective since the *para* substitution seems to favour better delocalization within the π-conjugated system.

Incorporation of a stronger electron-donating group like *p*-methoxy (σ_p = -0.27) leads to BbF **5** being only slightly easier to oxidize (1.31, 1.46 and 1.54 V) compared with reference **1**, but less than in the case of ^{t}Bu substituted **4**. In a similar fashion to compounds **2** – **4**, reduction processes of **5** are also easier to access by DPV (-0.64, -1.49 and -1.52 V) compared to **1** even though cyclic voltammetry seems to indicate a more difficult first reduction (-0.70 V [164 mV]). These results are rather surprising since significantly better π-electron delocalization throughout the whole system in BbF **5** was found both by X-ray structural data and theoretical calculations. In fact, the dihedral angle between the proximal aryl and the pyrrole was smaller [$\varphi_{C12-C13-C14-C15}$ of -18.9(4) / +11.6(3)° *vs.* -34.6(2)° for **1** by X-ray; 30.95° *vs.* 34.74° for **1** and 33.03 for **4** by DFT] in addition to the smaller tilt angle between the planes of the pyrrole and the benzo[b]-fused pyrrole [10.3(1) *vs.* 15.3(1)° for **1** by X-ray]. Furthermore, a higher dipole moment was calculated (7.26 D *vs.* 5.96 D for **4** and 6.39 D for **1**) that should affect the redox potentials as well. A possible explanation lies in the strong H-bonding regime observed in BbF **5** that may alter the reorganizational energy needed to stabilize charges during redox processes. In the case of BbF **8** bearing the strongest electron-donating group of the series, the dimethylamine substituent (σ_p = -0.83), the first oxidation is much easier to access at 0.88 V. A comparison with its closest analogue, *N,N*-dimethylaniline (0.80 V), suggests that the facile oxidation is due to the substituent itself.[63] The facile oxidation of the dimethylaminophenyl group also has implications in the emission spectroscopy as discussed later. The first reduction of **8** is more difficult (-0.79 V) *vs.* BbF **1**, as can be expected. This result combines effects of the strong electron donation of

dimethylamine with the most planar π-conjugated system of the series (tilt angle between pyrrole and benzo [b]-fused pyrrole planes of 4.2(1)° by X-ray and 7.5° by DFT; $\varphi_{C12\text{-}C13\text{-}C14\text{-}C15}$ = -27.7(2)° by X-ray and 24.75° calculated). A much stronger and quasi-perpendicular dipole moment (7.68 D) relative to **1** is also found. The presence of such an electron-rich group and improved conjugation allow the system to tolerate a total of four oxidized states within the CH_2Cl_2 potential window (0.88, 1.40, 1.50 and 1.68 V) related to both the dimethylamine itself and the dipyrromethene core. In addition to the first reduction, BbF **8** has two other processes at -1.57 and -1.64 V.

Introducing a methoxy substituent at the *meta* position of the aryl is expected to make it an electron-withdrawing group by induction (σ_m = +0.12) and should result in more positive oxidations and less negative reductions if the proximal aryl and the benzo[b]-fused DPM core are fully conjugated. Less positive oxidation processes are instead observed for BbF **6** (1.28, 1.39 and 1.54 V) bearing one *meta*-methoxy group as compared to **1**. Actually, the ease of oxidation provided by the *meta*-methoxy is even greater than for the *para*-methoxy substituted BbF **5** regarding the first and second oxidations. The first two reductions (-0.67 and -1.58 V) are nearly equivalent to what was observed for **1**, whilst the third one at -1.67 V is less negative by 0.11 V. All three reductive processes are, however, more negative than in the case of **5**, against what would be expected. Adding a second methoxy substituent in *meta* position leads BbF **7** to exhibit a significantly stabilized oxidative process at 1.39 V, as expected from computational studies, and is a 0.11 V positive shift compared to BbF **6** and 0.06 V from **1**. The origin of the oxidative processes might be altered as described previously for **8** since **7** only has a single oxidation compared to three for **5** and **6** and the value at 1.39 V match the second oxidative process of **6**. The reduction processes for BbF **7** (-0.65, -1.54 and -1.58 V) are easier to access than for **1** and **6**. Therefore, it appears the peculiar behaviour of BbF **6** and **7** relative to the reference **1** and closely

related **5** cannot be described by the sole electron donating / withdrawing propensity of the substituent. The logic behind rather resides in a combined effect with three other factors previously exposed, i.e. a weaker communication through the π-conjugated system (φ = 35.24° with one node on meta carbon for **6**; φ = 36.10° with two nodes for **7**) allied with the alteration of dipole moments (5.42 and 4.91 D, respectively) and potentially weaker H-bonding relative to BbF **5** as described in the X-ray section.

Extension of the π-electron conjugation path by fusion of cycles on the proximal aryl promises interesting effects since a complex system is at play, with inter-correlated factors dictating the experimental properties. BbF **9** combines both a 2-naphtyl unit and an electron-rich 6-methoxy substituent equivalent to the *para*-substitution of a single phenyl through mesomerism. In principle, this should provide redox processes that are easier to access as compared to reference **1**. Indeed, the results are as expected, with easier oxidations (1.26, 1.40 and 1.50 V) and reductions (-0.65, -1.51 and -1.55 V). Full expression of the substituent effect occurs due to the small calculated dihedral angle of 31.72° that promotes delocalization of the π-electrons combined with the largest dipolar moment of the series (7.73 D). However, this is not the case with BbF **10** for which the large calculated dihedral angle of 55.46° caused by steric hindrance almost completely inhibits the communication between the 9-phenanthrene moiety and the benzo[*b*]-fused DPM core. A slight orbital overlap between the two fragments still persists in the HOMO that maintains a minimal electronic connection as can be appreciated in Figure 5. The dipole vector is mainly translated compared to **1**, with a slightly shorter modulus (6.16 *vs.* 6.39 D, respectively). Altogether, oxidations processes are found at more positive potentials (1.40, 1.58 and 1.65 V) compared to **1**, whereas reductions become even easier (-0.64, -1.52, -1.58 V).

Conversion of the first oxidation and reduction potentials obtained by electrochemistry into eV is relevant in order to establish the energy level of the HOMO and LUMO frontier

molecular orbitals and to evaluate if the benzo[*b*]-fused BODIPYs reported herein meet the specific requirements for multiple applications (*vide supra*; Table 2 and Figure 2). A common requirement in all types of applications is to present a HOMO below the oxidation threshold established at -5.27 eV,[58] which is the case for the whole BbF series. Results indicate that the HOMO is in the range of -6.34 for **7** and **10** up to -5.82 eV for **8**, therefore, they are air stable. For photovoltaic applications, exact positions of the LUMO and the excited state oxidation potentials ($E_{Ox}*$) are required to ensure proper electronic transfers between the acceptor and the donor components of the studied system.[64] It was found that LUMO levels are in the range of -4.34 eV for **4** up to -4.15 eV for **8**, with $E_{Ox}*$ between -4.30 eV for **7** and **10** up to -4.05 eV for **8**. These values suggest that all derivatives in the BbF series present the possibility to be integrated into photovoltaic devices since both their LUMOs and $E_{Ox}*$, or at least the latter, are lying slightly above the LUMO of the main acceptor used in OPV [fullerene-based $PC_{60}BM$ (between -3.91 and -4.3 eV)][65] or of the TiO_2 conduction band (-4.2 eV)[66] used in DSSC. Interestingly, further fine-tuning can be achieved in OPV through careful selection of alternative acceptor materials that would provide the optimal driving force of about 0.3 eV suitable for good exciton dissociation into a pair of charges at the D – A interface.[67-75] Of all derivatives, BbF **8** bearing the NMe_2 group appears to be the best candidate for photovoltaic based on the highest lying LUMO / $E_{Ox}*$ and the smallest ΔE_{Ox} (1.67 eV) / ΔE_{Opt} (1.77 eV) that allow for harvesting of low energy photons.[3]

Table 2 – HOMO / LUMO levels (in eV) as determined by electrochemistry and theoretical calculations along with corresponding ΔE and estimated excited state oxidation potential (E_{ox}*) for BbF **1 – 10**.[a]

	HOMO redox	LUMO redox	ΔE_{Ox}	E_{Ox}*	HOMO theo	LUMO theo	ΔE_{Theo}
1	-6.27	-4.28	1.99	-4.20	-6.13	-3.23	2.90
2	-6.31	-4.31	2.00	-4.26	-6.07	-3.20	2.87
3	-6.28	-4.27	2.01	-4.23	-6.07	-3.20	2.87
4	-6.22	-4.34	1.88	-4.16	-6.07	-3.20	2.87
5	-6.25	-4.31	1.95	-4.22	-5.94	-3.14	2.80
6	-6.22	-4.28	1.94	-4.16	-6.13	-3.22	2.91
7	-6.34	-4.30	2.04	-4.30	-6.12	-3.21	2.91
8	-5.82	-4.15	1.67	-4.05	-5.51	-3.00	2.51
9	-6.20	-4.29	1.91	-4.23	-5.86	-3.19	2.67
10	-6.34	-4.31	2.03	-4.30	-6.07	-3.22	2.85

[a] Energy difference (ΔE, in eV) between the HOMO and the LUMO using corresponding method. Theoretical calculations using r-PBE0/6-311g(2d,p) DFT method with PCM = CH_2Cl_2. Estimated excited state oxidation potential calculated using: E_{ox}* = E_{Ox} + ΔE_{Opt}.

Figure 2 – Energy levels of BbF **1 – 10** (electrochemistry in black, DFT calculations in red and

corresponding ΔE at the bottom ; estimated excited E_{ox}* in blue).
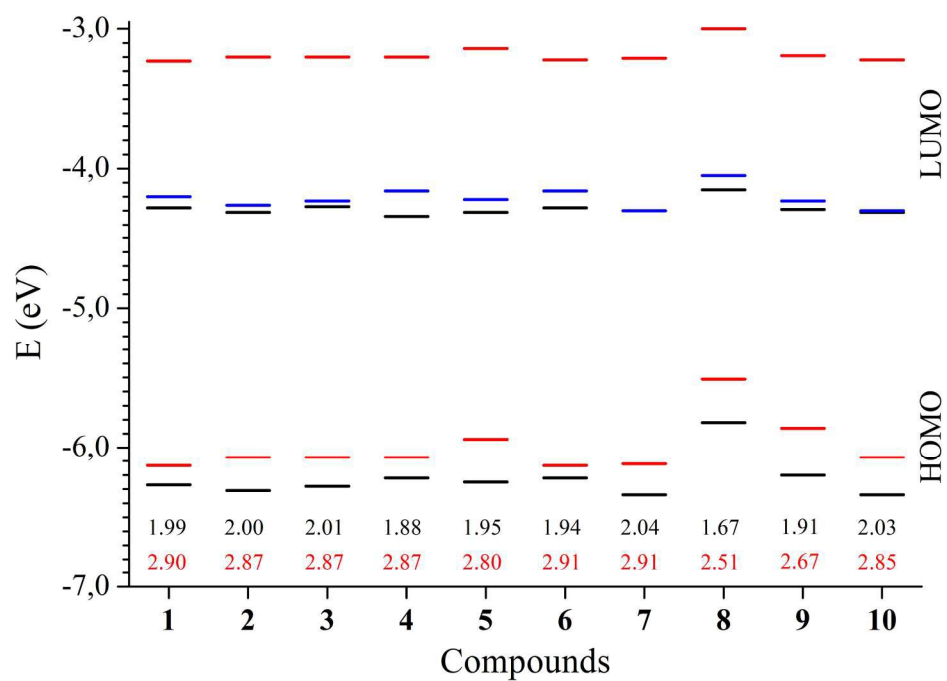
Red absorption and NIR emission properties

Spectroscopic data for the series are summarized in Table 3 and Figure 3, while individual spectra can be found in the ESI (Figures S.25 – S.41†). Overview of the photophysical properties of the BbF series in CH_2Cl_2 solution reveals a strong absorption of red light (λ_{red} = 547 – 626 nm; extinction coefficients (ε) = 36 – 57 x 10^3 M^{-1} cm^{-1}) complemented mainly by four other absorption bands of lower intensity, along with a relatively weak fluorescence (Φ_F = <0.01 – 0.11) spanning the deep-red to NIR parts of the electromagnetic spectrum (λ_{Em} = 606 – 757 nm; broad emissions from *ca.* 560 up to 875 nm). Such tuneable properties are highly desirable for various applications (*vide supra*) and the series will be further analyzed by TD-DFT in the computational modelization section and herein relative to previously reported BODIPYs (refer to Figure 1 and Table S.1†; in CH_2Cl_2 unless otherwise stated) in order to gain a better understanding of the impact of fusion modes and substitution on the rings.

Looking first at absorption spectroscopy, reference BbF **1** presents its lowest energy band at 553 nm (ε = 52 x 10^3 M^{-1} cm^{-1}) in dichloromethane that is bathochromically shifted by +49 nm *vs.* both the basic BODIPY core **22** (λ_{red} = 504 nm; ε = 14 x 10^3 M^{-1} cm^{-1}) and *meso*-phenyl substituted **23** (λ_{red} = 504 nm; ε = 58 x 10^3 M^{-1} cm^{-1}) measured in chloroform.[59] The solvatochromic effect on the λ_{red} between CH_2Cl_2 and $CHCl_3$ appears to be relatively negligible since **23** in DCM is at 500 nm (ε = 33 x 10^3 M^{-1} cm^{-1}), but the decrease in solvent polarity tends to diminish the extinction coefficient.[76] Therefore, the benzo[*b*]-fused chromophore **1** with a rigidified structure presents significantly improved photophysical properties compared to related BODIPYs **22** and **23**. This +49 nm bathochromic shift is also of the same magnitude to what can be observe by altering the *meso* carbon with a nitrogen atom in azadipyrromethene (ADPM) and Aza-BODIPY.[35, 39] When methyl groups are installed at the proximal and distal positions of the

BODIPY core in **24** (λ_{red} =501 nm; ε = 87 x 10^3 M^{-1} cm^{-1}), only a +1 nm shift is observed *vs.* **23**.[77]

Figure 3 – UV/vis absorption spectra of BbF **1 – 4** (top) and **5 – 10** (middle) and their normalized emission profiles (bottom) in CH_2Cl_2 solution.
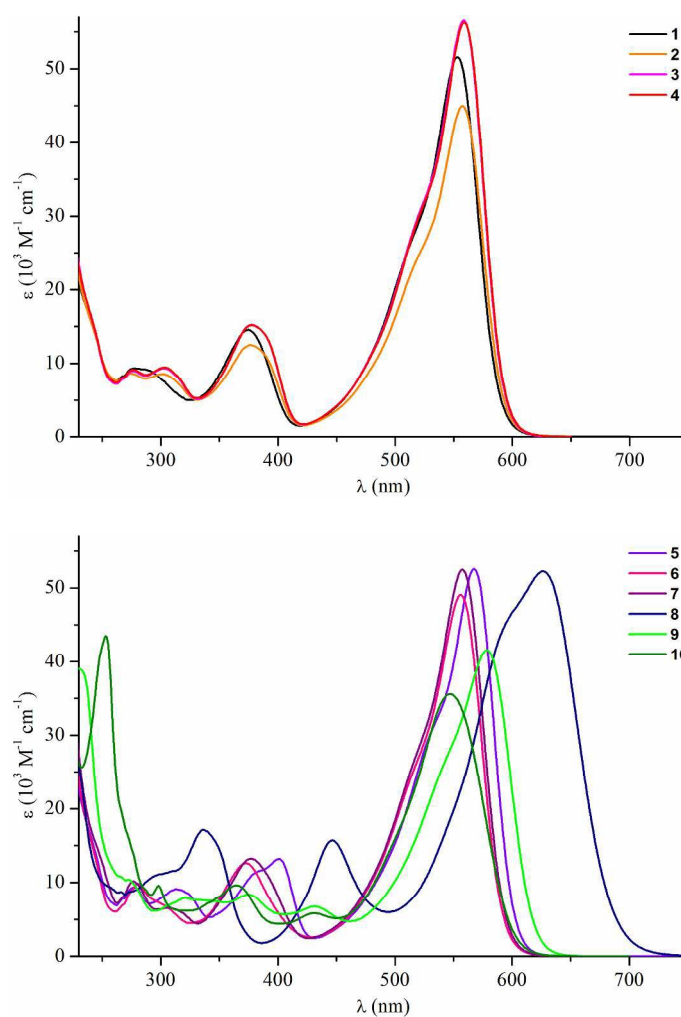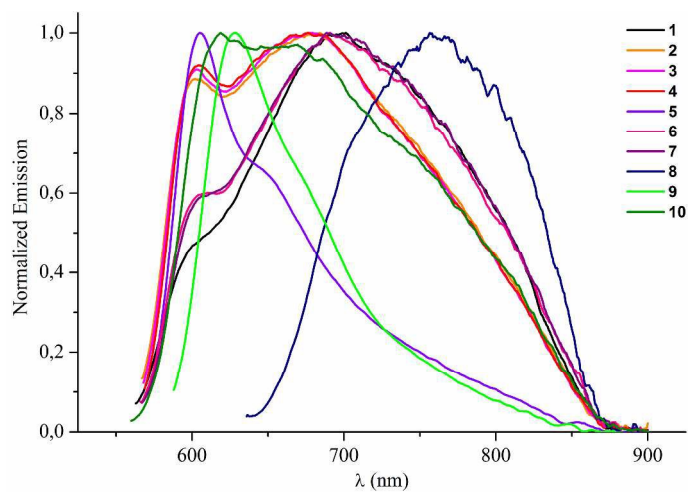
Table 3 – Photophysical properties of BbF **1 – 10**.[a]

	Absorption [a]							Emission [b]					
	λ_{UV}	$\lambda_{near\ UV}$	λ_{violet}	$\lambda_{sh\ orange}$	λ_{red}	ΔE_{Opt} (eV)	$\lambda_{red\ theo}$ [c]	λ_{Em}	FWHM	Δ_{Stoke} (cm^{-1})	Φ_F	τ (ns)	k_r / k_{nr} (10^9 s^{-1})
1	277 (9.3)	287 (9.2)	374 (15)	517 (28)	553 (52)	2.07	479 (0.939)	701	205	3818	< 0.01	0.48	0.02 / 2.1
[d]	274 (7.6)	282 (7.6)	373 (12)	513 (24)	545 (39)	2.10	---	734	256	4725	< 0.01	0.17	0.06 / 5.8
2	275 (8.6)	302 (8.6)	377 (12)	521 (25)	557 (45)	2.05	484 (0.987)	684	207	3333	0.02	0.59	0.03 / 1.7
3	276 (9.0)	303 (9.3)	378 (15)	523 (31)	558 (57)	2.05	484 (1.01)	679	207	3193	0.02	0.58	0.03 / 1.7
4	277 (9.1)	303 (9.5)	378 (15)	525 (32)	559 (56)	2.06	485 (1.01)	677	204	3118	0.01	0.56	0.02 / 1.8
5	278 (9.4)	314 (9.1)	401 (13)	537 (33)	567 (53)	2.03	495 (1.05)	606	88	1135	0.05	0.78	0.06 / 1.2
[d]	276 (10)	311 (9.7)	397 (14)	531 (37)	559 (54)	2.06	---	601	115	1250	< 0.01	0.22	0.05 / 4.5
6	281 (9.8)	303 (6.9)	373 (13)	520 (27)	556 (49)	2.06	479 (0.946)	691	222	3514	0.01	0.50	0.02 / 2.0
7	277 (10)	307 (6.5)	377 (13)	522 (29)	557 (52)	2.04	477 (0.942)	689	216	3439	0.01	0.50	0.02 / 2.0
8	301 (11)	336 (17)	446 (16)	597 (46)	626 (52)	1.77	542 (1.18)	757	149	2764	< 0.01	< 0.1	---
[d]	311 (13)	336 (20)	444 (16)	595 (53)	615 (57)	1.78	---	---	---	---	----	---	---
[e]	---	283 (16)	379 (15)	522 (29)	555 (54)	2.07	---	---	---	---	---	---	---
[f]	---	282 (17)	400 (16)	518 (36)	550 (60)	2.03	---	---	---	---	---	---	---
9	272 (10)	321 (7.9)[g]	431 (6.7)	548 (28)	578 (42)	1.97	511 (1.20)	628	87	1377	0.11	0.85	0.13 / 1.0
[d]	268 (11)	319 (7.5)[h]	426 (6.4)	536 (25)	569 (37)	2.03	---	632	116	1752	0.01	0.22	0.05 / 4.5
10	273 (16)	298 (9.5)[g]	431 (5.8)	511 (20)	547 (36)	2.04	491 (0.901)	619	196	2127	< 0.01	0.39	0.03 / 2.5
[d]	284 (10)	296 (11)[h]	426 (6.4)	502 (23)	536 (40)	2.10	---	592	230	1765	< 0.01	< 0.1	---

[a] Acquired at 25 ± 1 °C in CH$_2$Cl$_2$, otherwise stated. λ in nm. Extinction coefficients are given in parentheses (ε, x10^3 M^{-1}cm^{-1}). Shoulder = sh. ΔE$_{Opt}$ qualitatively obtained from the red end of the Gaussian peak of λ$_{red}$ (in nm) and converted into eV using E = hc / λ. [b] Emission maximum (λ$_{Em}$) obtained by excitation at corresponding λ$_{red}$. Full width at half-maximum (FWHM) in nm. Fluorescence quantum yields (Φ$_F$) obtained on a calibrated integration sphere. Fluorescence lifetime (τ) upon excitation by a pulsed laser at 405 nm (Standard deviation ≤ 0.02 ns). Radiative (k$_r$) and non-radiative (k$_{nr}$) rate constants were calculated using: k$_r$ = Φ$_F$ / τ and k$_{nr}$ = (1-Φ$_F$) / τ. [c] TD-BMK/6-311+G(2d,p); PCM = CH$_2$Cl$_2$. Oscillator strength given in parenthesis. Full assignation of the absorption bands available in the ESI. [d] In acetonitrile. [e] In CH$_2$Cl$_2$ with an excess of HClO$_4$. [f] In acetonitrile with an excess of HClO$_4$. [g] Another absorption band observed at 375 nm (ε = 8.3x10^3 M^{-1}cm^{-1}) for **9** and at 365 nm (ε = 9.6x10^3 M^{-1}cm^{-1}) for **10**. [h] Another absorption band observed at 373 nm (ε = 8.3x10^3 M^{-1}cm^{-1}) for **9** and at 364 nm (ε = 11x10^3 M^{-1}cm^{-1}) for **10**.

The closest family of non-symmetric dyes without the benzo[*b*]-fused moiety is the series **25 – 29** that was studied by the groups of Boens and Dehaen in acetonitrile (ACN).[78, 79] It will be discussed later in this section compared to their corresponding BbF in ACN, but it can already be noted that implementation of the benzo[*b*]-fused moiety provide an intrinsic red-shift of +22 nm (545 nm for **1** *vs.* 523 nm for **25**). Relative to closely related non-symmetric benzo[*b*]-fused derivatives **30** (λ_{red} = 512 nm; ε = 42 x 10^3 M^{-1} cm^{-1}) and **31** (λ_{red} = 539 nm in THF; ε = 54 x 10^3 M^{-1} cm^{-1}),[42, 48] it can be outlined that the presence of the unhindered proximal phenyl in BbF **1** contributes more significantly to reduce the HOMO-LUMO gap than does a methyl or a sterically crowded mesityl, both of which diminish the conjugation. Similarly, aryls installed on their indole moiety appear to have less effect on the resulting λ_{red} than the proximal phenyl does in **1**. These two last observations further support our initial hypothesis that the proximal aryl can provide significant leverage for modulation of the optoelectronic properties. Adding a second benzo[*b*]-fused moiety and two phenyls on the free indolic positions in symmetric derivative **32** further extends the π-conjugated system and allows the λ_{red} to be shifted by +15 nm, up to 568 nm, but at the price of a decreased extinction coefficient (42 x 10^3 M^{-1} cm^{-1}).[48] Fusing the benzene at the [*a*] bound in non-symmetric derivative **33** provide a λ_{red} at 570 nm, but present the major drawback of a free pyrrole in proximal position prone to unwanted side-reactions or degradation, especially in biological environment.[80] More stable symmetric benzo[*a*]-fused derivative **34** present interesting photophysical properties (λ_{red} = 631 nm; ε = 102 x 10^3 M^{-1} cm^{-1}) while **35** substituted with two proximal *ortho*-methoxy phenyls shows an hypsochromic shift of -14 nm due to the steric hindrance with the fused aromatic groups (λ_{red} = 617 nm; ε = 108 x 10^3 M^{-1} cm^{-1}).[61] Nevertheless, non-symmetric BbF **1** is more red-shifted than other [*b*]-fused moieties such as furan-based Keio Fluor **36** (542 nm in CHCl$_3$; ε = 140 x 10^3 M^{-1} cm^{-1}) and coumarin-

based **44** (516 nm; ε = 36 x 10^3 M^{-1} cm^{-1}).[81, 82] Pyridone-[*b*]-fused **45** reaches out to 578 nm (ε = 105 x 10^3 M^{-1} cm^{-1}),[83] but a push-pull motif between the electron-rich pyridone moiety on one side and the electron-poor ester on the other makes it difficult to assess clearly if the higher bathochromic shift observed *vs.* **1** is solely due to the fusion mode. Adding a zig-zag fusion to the benzo[*b*]-fused moiety in **42** leads to a -35 nm hypsochromic shift of the maxima of absorption (518 nm; ε = 56 x 10^3 M^{-1} cm^{-1}) *vs.* the BbF of reference combined with a broad tailing towards the NIR centered at *ca.* 770 nm.[48] Interestingly, a combination of benzo[*a*]-fused and imbricated carbazole moiety in BODIPY derivative **43** (482 nm; ε = ~55 x 10^3 M^{-1} cm^{-1}) absorbs at shorter wavelength in the red than the reference BbF **1**.[84] This is unexpected as each of the underlying modes of ring fusion taken separately point towards an increased bathochromic shift, i.e. symmetric benzo[*a*]-fused **34** absorbs further than its benzo[*b*]-fused counterpart **32** and zig-zag-fused **42** gives a tailing in the NIR. Overall, it appears not all the modes of ring fusion are equivalent and their interplay might provide counterintuitive effects on the photophysical properties.

As it was previously exposed with electrochemistry, the various substituents used in the BbF series provide a mean to considerably modulate their properties. The effect of the various alkyl chains in *para* position of the proximal aryl allows a tuning by +4 − 6 nm of the λ_{red} compared to BbF **1**; with **2** at 557 nm (Me; ε = 45 x 10^3 M^{-1} cm^{-1}), **3** at 558 nm (^{i}Pr; ε = 57 x 10^3 M^{-1} cm^{-1}) and **4** at 559 nm (^{t}Bu; ε = 56 x 10^3 M^{-1} cm^{-1}). This bathochromic trend is in line with the sequence of electron-donating alkyl groups and extended conjugation discussed earlier, albeit within experimental error. BbF **5** bearing the proximal *p*-OMe-Ph exhibits red shift of +14 nm *vs.* reference **1**, with λ_{red} at 567 nm (ε = 53 x 10^3 M^{-1} cm^{-1}). Interestingly, substitution in *meta* position with one methoxy group in **6** (λ_{red} = 556 nm; ε = 49 x 10^3 M^{-1} cm^{-1}) or two in **7** (λ_{red} =

557 nm; $\varepsilon = 52 \times 10^3$ M^{-1} cm^{-1}) doesn't provide the expected hypsochromic shift, rather moving the maxima of absorption respectively to +3 and +4 nm *vs*. **1**. The bathochromic shift observed for these EWG by induction is still much smaller than in the case of BbF **5** with electron-donation of the methoxy directly in the π-conjugated system. Again in the case of the photophysical properties, it appears the peculiar behaviour of BbF **6** and **7** relative to the reference **1** and closely related **5** cannot be described by the sole electron donating / withdrawing propensity of the substituent and must take into account the three other factors previously exposed in the electrochemistry section (extend of communication through the π-conjugated system; alteration of the dipole moment; strength of the H-bonding). As can be expected by structural characterization of BbF **8**, the presence of the strongly coupled EDG dimethylamine in *para* position leads to a significant +73 nm red-shift ($\lambda_{red} = 626$ nm; $\varepsilon = 52 \times 10^3$ M^{-1} cm^{-1}) which suggests a charge-transfer transition from the dimethylamine to the dipyrromethene core. Such a shift in the optical properties makes this BbF derivative highly suitable for photovoltaic applications.[3] Addition of an excess of $HClO_4$ in the UV cuvette instantly protonated the substituent ($NHMe_2^+$), leading to a drastic -71 nm hypsochromic shift of the λ_{red} (555 nm; $\varepsilon = 54 \times 10^3$ M^{-1} cm^{-1}) (Figure S.36) leaving the intrinsic absorption profile of the dipyrromethene core, supporting the assignment of this charge-transfer transition. The overall absorption profile also closely matches that of reference BbF **1**, proving retained structural integrity of the dye and its potential use as pH-sensitive probe. Extension of the π-conjugated system in 6-methoxynaphthalen-2-yl substituted BbF **9** ($\lambda_{red} = 578$ nm; $\varepsilon = 42 \times 10^3$ M^{-1} cm^{-1}) provides a +25 nm red-shift *vs*. **1**, which is an intermediate effect between the *p*-OMe-Ph BbF **5** and the *p*-NMe$_2$-Ph BbF **8**. Further extension of π-conjugated system with the 9-phenanthrene moiety leads to the only hypsochromic shift of the series, by 6 nm, clearly attributable to the poor communication

between this sterically crowded substituent and the BODIPY core (*vide supra*). Finally, a comparative overview of variously substituted Keio Fluors (KFL) **36** – **41** studied in CHCl$_3$ provide interesting information that can be extended to the BbF series.[81, 85] Going from the non-symmetric KFL **36** (λ_{red} = 542 nm) to the symmetric **37** (λ_{red} = 579 nm) gives a +37 nm bathochromic shift, which is as important as increasing the conjugation with additional phenyls in the symmetric KFL **38** (λ_{red} = 652 nm; +73 nm red-shift / *ca.* 36.5 nm per Ph). This trend is in accordance with the +11 nm shift obtained for BbF **9** *vs.* **5** (+25 nm *vs.* **1**), which disfavours the idea of replacing the proximal aryl in the series by alkyl chains for efficient absorption of deep-red light. Within the symmetric KFL derivatives, it is interesting to note that *para-^{i}*Pr-phenyls in **41** (λ_{red} = 662 nm) provide a bathochromic shift of +10 nm compared to **38** while *ortho*-OMe-phenyls give +19 nm in **40** (λ_{red} = 671 nm) and *para*-OMe-phenyls +21 nm in **39** (λ_{red} = 673 nm). When comparing the bathochromic effect per aryl obtained in KFL *vs.* their BbF counterparts, it is exactly the same for *^{i}*Pr-Ph (+5 nm) and slightly less important for *ortho* / *para* substituted KFL's (+9.5 / 10.5 nm) than in BbF **5** (+14 nm). This suggests that rational fine-tuning can be achieved when designing new BODIPYs, given that the substituents used will affect the conjugation pathways in a similar fashion.

As mentioned previously, a few derivatives of the BbF series were further studied in ACN solvent (Figures S.25, S.27, S.32, S.37, S.39 and S.41) in order to establish a better correlation with the unfused non-symmetric derivatives **25** – **29**.[78, 79] The direct comparison in ACN of BbF **1** and derivative **25** that are both equipped with a phenyl at the *meso* position shows that a red-shift of +22 nm is obtained by benzo[*b*]-fusion (λ_{red} = 545 and 523 nm, respectively). This shift also needs to be related to the +9 nm shift of **1** *vs.* BODIPY **26** bearing a sterically hindered and electron-poor *meso*-2,6-dichlorophen-1-yl moiety (λ_{red} = 536 nm). Since derivatives **27** – **29** also

have this last moiety, the reduction of 13 nm in the bathochromic shift of **26** *vs.* **25** needs to be kept in mind. From there, it can be seen that BbF **5** (λ_{red} = 559 nm) has only a shift of +5 nm *vs.* the unfused derivative **27** (λ_{red} = 552 nm) (+14 nm *vs.* **1**). For BbF **8** (λ_{red} = 615 nm), a shift of +7 nm *vs.* **28** (λ_{red} = 608 nm) is obtained (+70 nm *vs.* **1**). Hence, it can be noted from these comparisons implying BbFs **1**, **5** and **8** that substitution at the *para* position of the proximal aryl has less effect on the benzo[*b*]-fused system relative to the same substitution on the unfused pyrrole of compounds **27** – **29**. Interestingly, the authors behind the study of unfused systems also tested the addition of $HClO_4$ in excess to a methanolic solution of **28** and observed a similar blue-shift behaviour (-73 nm) from 608 nm back to 535 nm.[78] As it is insoluble in methanol, BbF **8** was further tested in ACN and protonation of the dimethylamine group provided a smaller hypsochromic shift of -65 nm, from 615 nm back to 550 nm. Non-symmetric derivative **29** (λ_{red} = 547 nm) allows a better evaluation of the sole effect of extending the π-conjugated system with a 2-naphthalen moiety. A red-shift of +11 nm is found compared to its proximal phenyl counterpart **26**, while BbF **9** (λ_{red} = 569 nm) reaches +24 nm *vs.* BbF **1**. Thus, addition of the methoxy group in **9** should provide a red-shift of about +13 nm compared to a related BbF bearing a simple naphthalene, which is consistent with the +14 nm shift obtained for BbF **5** *vs.* **1**. Even though the exact unfused counterpart was not available, we looked at BbF **10** (λ_{red} = 569 nm) to further probe if the more polar ACN medium would promote a better communication between the sterically hindering phenanthrene moiety and the adjacent pyrrole. A blue-shift of -9 nm compared to **1** is found in ACN, which is higher than the -6 nm obtained in DCM and indicate an overall destabilization. This investigation of the five BbF in ACN also ascertained that a moderate solvatochromic effect occurs when switching from the less polar DCM, with blue-shifted values between -8 nm for derivatives **1** and **5** up to -11 nm for **8** and **10**. BbF **9** presented

an intermediate shift at -9 nm. As a gauge, these values are about two-to-three times more appreciable than the -4 nm blue-shift encountered in the simpler BODIPY **24**.[86]

Emission properties of the non-symmetric benzo[*b*]-fused platform reported herein are highly promising due to the broad fluorescence in the NIR region (*vide supra*; Figure 3 bottom; Table 3) and large Stoke shifts (up to 3818 cm^{-1} in CH_2Cl_2 / 4725 cm^{-1} in ACN for BbF **1**). As it is expected from the free rotating *meso*-phenyl offering a major deactivation pathway of the excited state,[87] the quantum yields (Φ_F) obtained are rather low (BbF **1**, **8** and **10** below 0.01 and highest values reaching 0.05 for **5** and 0.11 for **9** in CH_2Cl_2 solution). For BbF **8**, this nearly non-fluorescent behaviour is expected due to low energy of the emission and potential quenching of the excited state by the dimethylamino group, as shown for compound **28**.[78] Indeed, apart from complex **8**, all of the complexes display both higher and lower energy emission bands assigned to the typical fluorescence of BODIPYs and to charge-transfer bands, respectively (Figure 4). The latter assignment is suggested by the broad nature of the emission bands between 684-757 nm and their strong dependence on solvent polarity. The emission is almost fully quenched in polar ACN solvent for the five BbF studied. The lifetimes are also very short in both solvents ($\tau < 1$ ns throughout the series) and leads to high non-radiative rate constants ($k_{nr} = 1.0 - 2.5 \times 10^9$ s^{-1} in DCM). However, this low Φ_F can easily be overcome by incorporating stoppers to the phenyl rotation either on the BODIPY core, *e.g.* **23** ($\Phi_F = 0.03$) *vs.* 1,3,5,7-tetramethyl substituted **24** ($\Phi_F = 0.67$) in DCM,[76, 77] or directly on the *meso* substituent, *e.g.* unfused derivative **25** ($\Phi_F = 0.02$) enlightens by substitution with the *meso*-2,6-dichlorophen-1-yl of **26** ($\Phi_F = 0.88$) in ACN.[78, 79] This assumption is even further supported by other unfused derivatives **27** ($\Phi_F = 0.85$) and **29** ($\Phi_F = 0.77$) bearing similar proximal substituents encountered in the BbF series and the versatile synthetic platform on which the latter is based (*vide supra*). Along this line, non-symmetric

benzo[*b*]-fused **30** equipped with both a phenyl and a methyl as blocking groups increased Φ_F up to 0.10 even though no proximal aryl group was installed.[48]

Computational Modelization Insights

Multiple parameters need to be considered when choosing a computational modelization method in order to find a good equilibrium between highly accurate results and the computational cost.[88-91] In the specific field of BODIPYs dyes and their related Aza-BODIPYs, significant efforts have been made recently by Jacquemin and coworkers to reach a good compromise.[92-95] Still, many different DFT protocols can be found within the field in order to predict or rationalize their optoelectronic properties.[42, 48, 84, 96-98] Based on our previous work with ADPM derivatives using a method developed by Jacquemin *et al.* for Aza-BODIPYs, we decided to use the TD-DFT // DFT protocol PCM-TD-BMK/6-311+G(2d,p) // PCM-PBE0/6-311G(2d,p) with the Polarization Continuum Model (PCM) of CH_2Cl_2 in order to gain insights on the molecular orbitals and structural properties of the BbF series by DFT along with the optical transitions involved by TD-DFT (refer to Computational Methods of ESI†).[39, 95] While this protocol presents inherent limitations due to the vertical approximation, it already proved to rapidly reach semi-quantitative estimates of the λ_{max} and to be flexible towards important structural changes (Aza-BODIPY *vs.* ADPM; various type of aryls in proximal and distal positions). The opportunity to further test this protocol by expanding it to BODIPYs, comparing the DFT structural optimization with crystallographic data and assessing the ability of TD-DFT to predict the relative order of λ_{max} within the BbF series thus became appealing.

As mentioned in the electrochemical section, structural information is essential to rationalize experimental results. The first step to ascertain the validity of the PCM-PBE0/6-

311G(2d,p) DFT method was to start the calculations from the crystallographic data obtained for the reference BbF **1** and to optimize it. The second step was to construct from these data other BbF of the series and compared their optimized structures with available crystallographic data for BbF **5**, **8** and **9** (Tables S.23 and S.24†). The result was a good matching of bond lengths *vs.* the X-ray data in atoms not directly implied in a structural modification, supporting that an appropriate DFT method was used. Planarization of the DPM core was calculated in all cases, which is generally offset from X-ray results. However, the method was still able to distinguish the better delocalization encountered in BbF **8**. Obviously, one also needs to consider the single molecule environment of theoretical calculations as opposed to the intermolecular forces taking place in the crystal packing in order to explain up to a certain extent the structural differences found. The main drawback of this method appears to be its inability to properly estimate the relative order in the strength of intramolecular H-bonding between the hydrogen on the *ortho* carbon of the proximal aryl and one of the fluoride atoms on the nearby BF_2 chelate (Tables S.25 and S.28†). Actually, the computation established that this H-bonding should theoretically be the strongest in BbF **8** where the *p*-NMe_2 is expected to provide the best conjugation with the pyrrole moiety to which it is attached. X-Ray crystal structure showed that this H-bonding is in fact less important than for *p*-OMe substituted BbF **5**, since two different H-bonds were possible in this specific derivative. As optimization explores the energy continuum around the starting geometry in order to find a well of stability, such a special case found in **5** couldn't be predicted by any computational methods. Therefore, the benchmarking of the DFT method used appears satisfactory for the BbF series investigated herein.

The frontier molecular orbitals are depicted in Figure 4 and the electronic distribution on the different fragments is given in Table S.2 and Figure S.62 of ESI†. Results show the HOMO is mainly located on the benzo[*b*]-fused DPM core and the proximal aryl, with almost no electronic

density on the *meso*-phenyl or the BF_2 chelate. The contribution of the *para* substituents on the proximal aryl increases with the strength of the EDG; 10% for reference **1**, 15% for alkyl substituted **2 – 4**, 28% for methoxy substituted **5** and 58% for **8** bearing the dimethylamine group. Introducing one or two methoxy groups in *meta*-positions leads to 13% in **6** and 12% in **7**, respectively, as anticipated from the EWG by an induction effect. Extending the π-conjugated system in **9** leads to 50% of electronic density being found on the 6-methoxynaphthalen-2-yl moiety. Only 34% of density is observed in **10** as expected from the bulky phenanthren-9-yl moiety which decreases communication with the adjacent pyrrole (*vide supra*). The empty LUMO presents an electronic redistribution mainly from the DPM core and proximal aryl towards the *meso*-phenyl and BF_2 chelate according to the same trend described in detail for the HOMO upon variation of the substituent. Therefore, calculations suggest that the indole moiety keeps its EWG character throughout the series as the electron-richness of the pyrrole is tuned by the proximal phenyl, reinforcing the idea of a push-pull effect within the BODIPY core.

Figure 4 – HOMO / LUMO (isovalue = 0.02), dipole moment vector (blue; modulus given in Debye) and dihedral angle (red; φ) between the proximal aryl and the DPM core of BbF **1 – 10** as obtained by DFT.
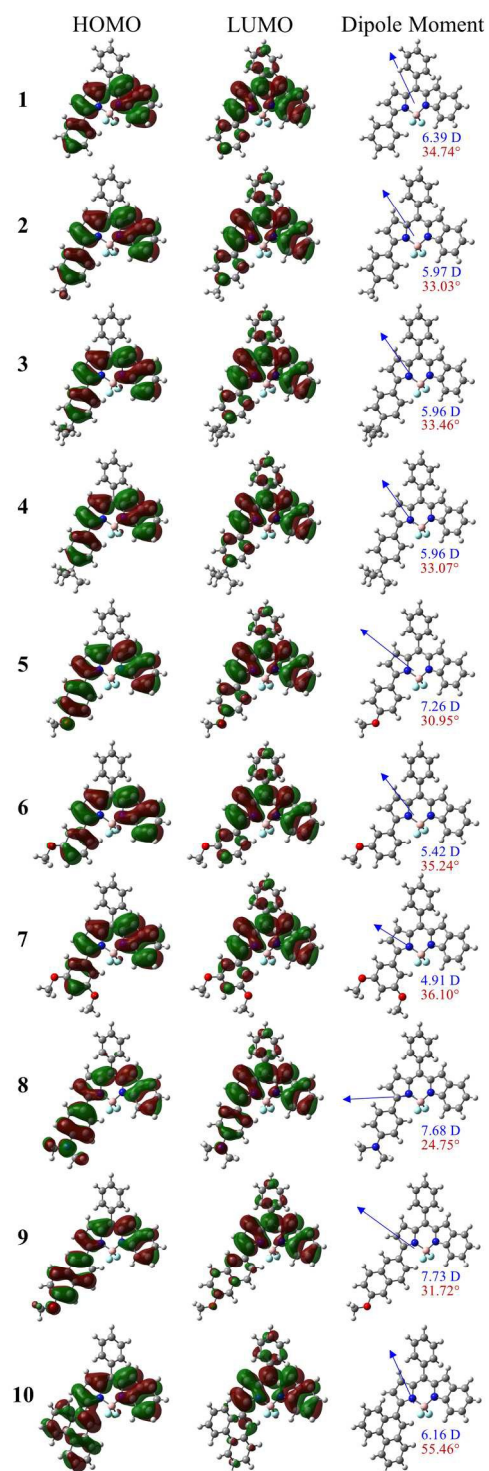
The dipole moment was found to be of great importance in the factors governing the electrochemical properties (*vide supra*). Calculations indicate that three key parameters are interplaying to modify the overall polarity of the molecule: i) the nature of the proximal substituent; ii) the degree of communication between the proximal aryl and the adjacent pyrrole; iii) the degree of communication within the benzo[*b*]-fused BODIPY core. Such information is thus critical to bear in mind when designing new dyes with specific electronic properties.

When comparing the energy levels obtained by computation *vs.* experimental ones (Figure 2 and Table 3), a few discrepancies are found. First, the DFT method tends to underestimate the variation in alkyl substituents on the HOMO and LUMO. Second, theoretical results for BbF **5** are offset since computation alone cannot account for the strong H-bonding regime providing two different molecular configurations and overriding the *para*-substitution trend effect. Third, the induction effect of the *meta*-methoxy substituted BbF **6** and **7** is poorly accounted for as compared to reference **1**. Still, a significant difference is correctly predicted for the HOMO between **7** and *para* substituted Bbf **5**. Fourth, DFT predicts a similar planarization of the benzo[*b*]-fused BODIPY core throughout the series with a tilt angle between planes of the pyrrole and the benzo[b]-fused pyrrole in the range of $8.6 - 8.9°$, an exception being that of BbF **8** at $7.5°$ (Tables S.23 and S.24†). This planarization was found to be much more variable in the available X-ray data (Table S.27†), ranging from $4.2°$ in **5** up to $15.3°$ in **1**. This difference suggests that in some cases computational analyses overestimate the overall communication of π-electrons between the different molecule's components and, therefore, the impact of the proximal aryl. Fortunately, the method was able to properly identify the more pronounced planarization effect of the *p*-NMe$_2$-Ph on the benzo[*b*]-fused BODIPY core in BbF **8**. It also provided a very good match with empirical results in the BbF **8** − **10** series, showing its reliability when strong EDG are used or when the conjugation between the proximal aryl and adjacent pyrrole is

sterically hindered. Altogether, care must be taken in the analysis of computational results when so many parameters are interplaying. This is especially important if the method is to be used *a priori* of the synthesis.

A complete analysis by TD-DFT of optical transitions for the BbF series in CH_2Cl_2 is provided in Figure 5, Table 3 and in the ESI† (Figures S.63 – S.72; Tables S.3 – S.22). The trend in $\lambda_{red\ theo}$ calculated is generally in excellent agreement with the empirical order. The method accounts for a red-shift of +5 – 6 nm in alkyls substituted derivatives **2** – **4** compared to reference BbF **1**, which was found to be of +4 – 6 nm for λ_{red}. Similarly, the calculated shift of +16 nm for BbF **5** is close to the empiric +14 nm. Inductive effect of the *meta*-methoxy groups is taken into account by the TD-DFT with a -2 nm hypsochromic shift for **7** and no shift for **6**, but empiric values were slightly red-shifted by +4 and +3 nm, respectively, compared to BbF **1**. Remarkably, the biggest calculated shift in the series was for BbF **8** (+63 nm), in accordance with the biggest one measured (+73 nm). The relative order of *p*-methoxyphenyl substituted **5** (+16 nm vs. **1**), 6-methoxynaphthalen-2-yl **9** (+32 nm; +25 nm observed) and *p*-dimethylaminephenyl **8** (+63 nm) was also properly modeled. The only major difference obtained was the predicted bathochromic shift of +12 nm for BbF **10** that was in fact found to be an hypsochromic one (-6 nm). Therefore, the PCM-TD-BMK/6-311+G(2d,p) protocol used provides reliable semi-quantitative trend with *para*-substitution and extended π-conjugated system where the steric hindrance is not too important.

The calculated transitions obtained by TD-DFT and Natural Transition Orbitals (NTO) analysis can help assign the observed absorption band in the BbF series.[99] The reference BbF **1** has a strong T1 transition (osc. strength = 0.939) corresponding to the λ_{red} at 553 nm which involves the HOMO -> LUMO orbitals at 99% (Figure 5 and Table S.3). This T1 transition is

constant throughout the whole BbF series **1 − 10**, with almost no orbital mixing encountered. Therefore, their λ_{red} can be illustrated by looking at the variation of electronic density between the HOMO and the LUMO in Figure 4. The shoulder in the orange part of the spectrum for **1** ($\lambda_{sh\ orange}$ = 517 nm) corresponds to the weak T2 transition (osc. strength = 0.015) where the electronic density upon excitation is mainly taken from the indole moiety towards the whole benzo[*b*]-fused BODIPY core and the proximal phenyl (HOMO-1 -> LUMO at 98%). At higher energy, λ_{violet} at 374 nm is attributable to a combination of T3 − T6 with mixed orbitals contributions from the proximal phenyl, the adjacent pyrrole and the *meso*-phenyl that are all heading to the LUMO upon photoexcitation. The absorption band $\lambda_{near\ UV}$ at 287 nm is another combination of transitions leading to the LUMO. In this case, T7 transfers density mainly from the proximal phenyl, the adjacent pyrrole and the *meso*-phenyl while T8 does it from the indole moiety. Beyond that point, highly energetic transitions in the UV region start to reach higher unoccupied orbitals such as in T9 (HOMO -> LUMO+1 at 84%) and T10 (HOMO -> LUMO+2 at 84%). These two last calculated transitions account for the λ_{UV} at 277 nm. An almost identical assignation as the reference **1** can be made for alkyl substituted BbF **2 − 4**, which is in accordance with the observed absorption spectrum at the top of Figure 3. The only significant difference regards the better definition of $\lambda_{near\ UV}$ at *ca.* 300 nm, which is due to the electron-donating properties of the alkyls providing a slight red-shift. *Para*-methoxyphenyl substituted BbF **5** has an apparent splitting of the λ_{violet} at 401 nm and *ca.* 380 nm. This is simply due to the increased oscillator strength of T4 (0.031 vs. 0.025 in **1**). Except this feature, the general absorption profile is very similar to previously discussed BbF **1 − 4**. Spectra of BbF **6** and **7** are alike, with a higher λ_{UV} absorption band *vs.* $\lambda_{near\ UV}$ that arises from the increased contribution of the *meta*-substituents in T9 and T10 associate with λ_{UV}. BbF **8** is of interest since $\lambda_{near\ UV}$ drastically

increases compared to reference **1** in addition to the expected red-shift of absorption maxima due to the strong EDG. This last band involves calculated transitions T4 – T6 where the proximal aryl, the adjacent pyrrole and the *meso*-phenyl all transfer their electronic density towards the LUMO. The general effect of extending the π-conjugated system of the proximal aryl in BbF **9** and **10** is a broadening of the absorption bands in the visible part of the spectrum (*ca.* 280 to 450 nm). For BbF **9**, the most significant impact of the extension is seen in T3, corresponding to λ_{violet}, and T4 associated with the new band at 375 nm. In BbF **10**, the impact is on transitions T3 – T5, with T3 corresponding to λ_{violet} plus T4 and T5 associated with the new band observed at 365 nm.

Overall, the semi-quantitative TD-DFT // DFT protocol used to rationalize the empirical results of electrochemistry and spectroscopy provided essential insights. Still, a critical analysis of the calculations compared to experimental measurements showed that the complex interplay of structural factors in the BbF series is hardly accounted *in silico* and precautions should be taken if modelization is to be made ahead of the synthesis.

Figure 5 – NTO analysis for absorption transitions T1 – T10 of reference BbF **1** (red =

calculated; green = corrected; grey = oscillator strength). Refer to ESI for a complete analysis of

the series.†
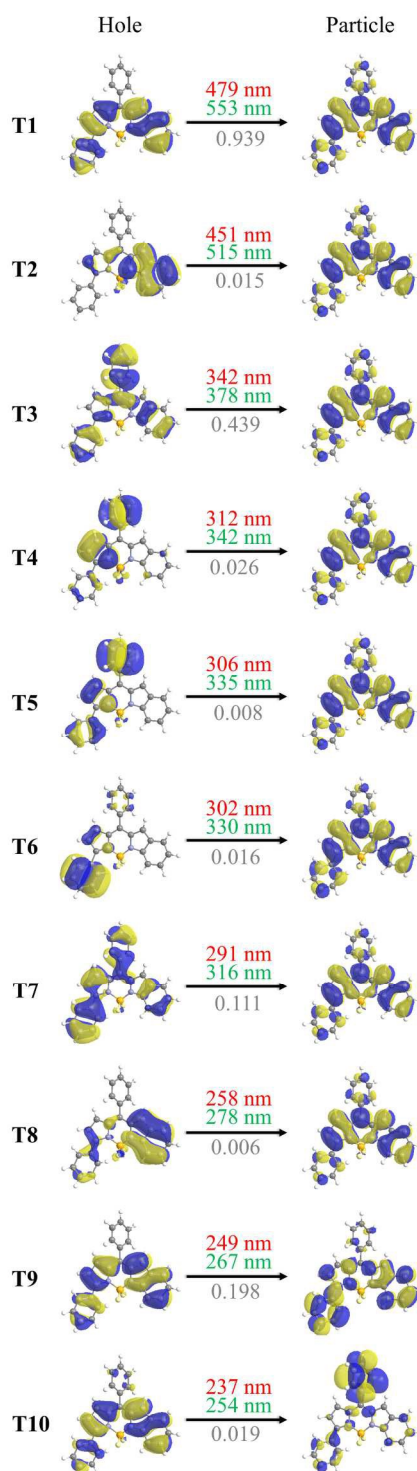
X-Ray Diffraction

Crystals suitable for X-ray diffraction studies were obtained for a good variety of substituents on the proximal aryl including the reference BbF **1** and *para*-substituted derivatives **5** equipped with a methoxy, **8** with a dimethylamine and **9** with the extended π-conjugated system of 6-methoxynaphthalen-2-yl (Figure 6 and Tables S.26 – S.28†). Compounds **1**, **8** and **9** crystallized in the orthorhombic crystal system (Pbca, $P2_12_12_1$ and $Pna2_1$ space groups, respectively) while **5** crystallized in the $P2_1/c$ space group (Table S.26†). The latter structure required additional refinement operations in order to model the disordered *p*-OMe-Ph moiety due to intramolecular hydrogen-bonding with both fluoride atoms acting as acceptors for a C-H donor in *ortho*-position of the proximal aryl group. Thus, two positions coexist for this substituent in a 53 : 47 ratio. While H-bonds were observed in all four complexes, only one hydrogen bond to a single fluoride atom was observed for **1**, **8** and **9** leading to no such disorder (Figure 6 and Table S.28†). According to the requirements of donor-acceptor distance and donor-H-acceptor angles for strong H-bonding (D···A = 2.5 – 3.2 Å / D-H···A = 130 – 180°),[100] it was found that all four compounds fall within this regime. However, only BbF **5** is within the expected range for strong H-bonds regarding H-acceptor distances (H···A = 1.5 – 2.2 Å), with values of 2.080(1) and 1.933(1) Å for the two disordered positions. BbF **8** is slightly longer [2.227(1) Å] to be considered in the strong regime, while a larger deviation is observed for reference **1** and **9** [2.352(1) and 2.351(1) Å, respectively]. Investigation of the core structure shows that the introduction of the benzo[*b*]-fused pyrrole favours the resonance form with the benzene being aromatic and nonaromatic azafulvene substructures (as depicted in Scheme 1) over a quinoidal structure of the indole moiety, at least in the solid-state. Supporting this, C1-N1 is longer than C13-N2 [1.372(2) – 1.378(2) *vs.* 1.347(2) – 1.359(2) Å] and C8-C9 is longer than C9-C10 [1.425(2) – 1.432(2) *vs.* 1.381(2) – 1.384(3) Å] in all four compounds (Table S.27†). A similar

observation was reported by Wakamiya *et al.* for the non-symmetric benzo[*b*]-fused BODIPY **31** (Figure 1) and further calculations suggested the quinoid form also contributes to some extent to the resonance equilibrium.[42] The tilt angle between the pyrrole ring and its benzo[*b*]-fused pyrrole counterpart also helps understand the extent of conjugation within the DPM core itself. The bottom of Figure 6 shows that this angle is much smaller in the case of BbF **8** [4.2(1)°] than for **9** [9.9(1)°], **5** [10.3(1)°] or the reference **1** [15.3(1)°]. Thus, the electron delocalization efficiency follows the same trend with **8** having the most conjugated core and **1** the least.

No other significant variation (within 3σ) on bond lengths or angles was found except in the case of BbF **8** for which the C13-C14 bond connecting the proximal aryl substituent to the pyrrole ring is shorter than in other BbF derivatives [1.452(2) *vs.* 1.466(2) – 1.470(2) Å], indicating some double-bond character and an increased communication between the π-electrons of the two fragments. This was also supported by the shorter C17-N3 distance [1.358(2) Å] as compared to *N,N*-dimethylaniline [1.385(4) Å].[101] The dihedral angle between the proximal aryl and the pyrrole ring (C12-C13-C14-C15) in **5** exhibits the smallest angles [-18.4(4) and +11.6(3)° for the two disordered positions] as compared to **8** [-27.7(2)°], **1** [-34.6(2)] and **9** [+39.5(3)°] in increasing order. This trend is consistent with the short intramolecular H-bonding distance in the solid-state, i.e., compound **5** displays the shortest H-to-F distance consistent with a strong C-H to F hydrogen bond, and therefore, the lowest tilt angle of the solid-state structures. The tilt angles between the *meso*-phenyl and the DPM moiety display less deviation, with absolute values between 47.4(1)° for **9** and 52.2(1)° for **8**. Interestingly, BbF **9** crystallized with both the proximal aryl and *meso*-phenyl in opposite directions as compared to related derivatives.

Together, these structural results revealed a significant interplay in the degree of communication between the proximal aryl, the pyrrole to which it is attached and the adjacent

indole moiety which is in agreement with electrochemical, photophysical and theoretical data previously discussed.

Figure 6 – Solid-state structures of BbF **1** (R$_1$ = 4.88 %), **5** (5.04 %)**, 8** (2.77 %) and **9** (3.04 %). [Ellipsoids shown at 50 % probability level; intramolecular H-bonds represented in dot grey; dihedral angles defined in red, angle between pyrrole and indole planes (bottom)].
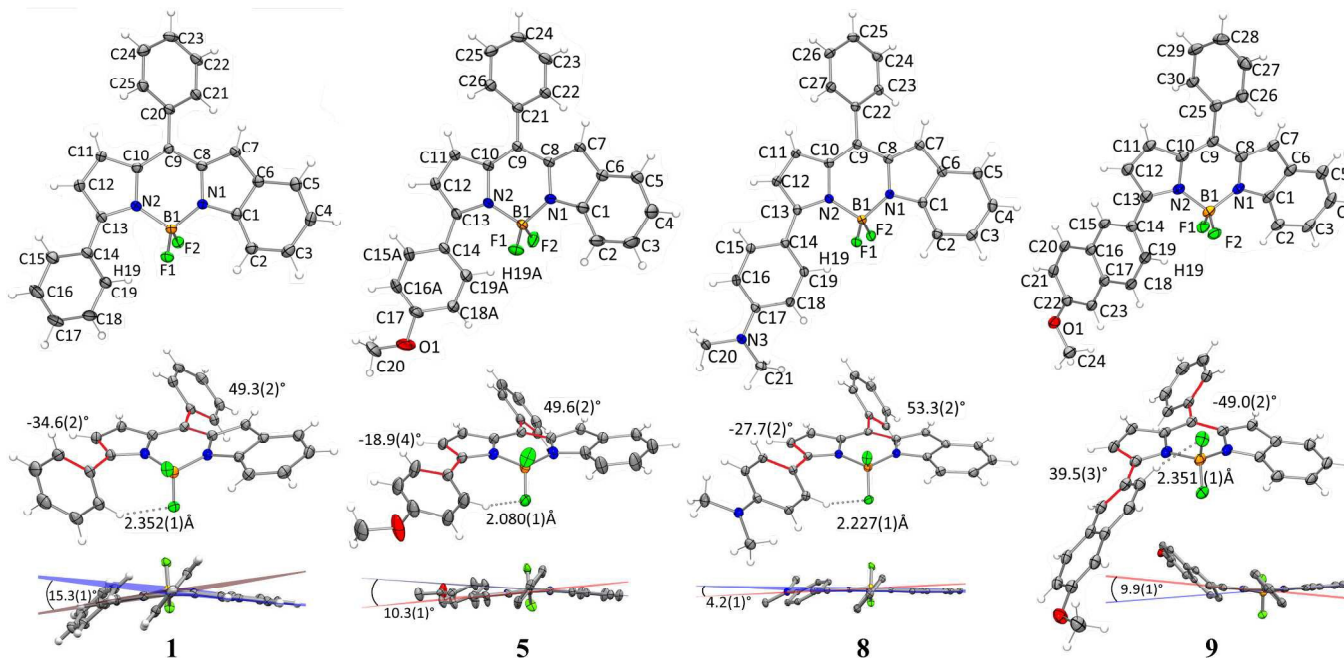
CONCLUSION

In summary, a novel family of ten non-symmetric benzo[*b*]-fused BODIPYs bearing various proximal aryls was prepared according to a versatile synthetic method. A critical analysis compared the optoelectronic properties obtained within the BbF series and across an extensive series of 23 derivatives from 9 different BODIPY families. Such an exercise provides a better overview of the impact of various fusion modes and π-system modifications available for BODIPYs and may provide guidelines for the design of new fluorophores specifically tailored for the plethora of applications where these compounds are now applied. Along this line, the non-symmetric BbF platform reported herein was discussed regarding the requirements for photovoltaic component and molecular probes. Adduct **8** was shown to be especially interesting for both type of applications. X-Ray structural characterization and computational modelization were further used to gain insights on the properties observed by electrochemistry and spectroscopy. In order to assess the validity of the computational protocol used and to evaluate its potential as a reference, it was compared to the structural data obtained by crystallography and other experimental measurements. Overall, the BbF platform proves to be a powerful one as it offers considerable leverage for efficient fine-tuning of optoelectronic properties and applications as efficient deep-red absorbers and NIR fluorophores.

ASSOCIATED CONTENT

Supporting Information

Experimental section including materials, instrumentation and synthetic methods; NMR; MS; electrochemical and spectroscopic details; computational methods and results; crystallographic data for BbF **1**, **5**, **8** and **9** (CCDC 1418610 – 1418613).

AUTHOR INFORMATION

Corresponding Author
* E-mail: garry.hanan@umontreal.ca ; Fax: +1 514 343 7586; Tel: +1 514 340 5156.

ACKNOWLEDGEMENTS

Dalton Transactions Accepted Manuscript

REFERENCES

1.　A. Loudet and K. Burgess, *Chem. Rev.*, 2007, **107**, 4891-4932.
2.　R. Ziessel, G. Ulrich and A. Harriman, *New J. Chem.*, 2007, **31**, 496-501.
3.　A. Bessette and G. S. Hanan, *Chem. Soc. Rev.*, 2014, **43**, 3342-3405.
4.　G. Ulrich, R. Ziessel and A. Harriman, *Angew. Chem., Int. Ed.*, 2008, **47**, 1184-1201.
5.　H. Lu, J. Mack, Y. Yang and Z. Shen, *Chem. Soc. Rev.*, 2014, **43**, 4778-4823.
6.　A. Mishra and P. Bäuerle, *Angew. Chem., Int. Ed.*, 2012, **51**, 2020-2067.
7.　S. K. Balasingam, M. Lee, K. Man Gu and Y. Jun, *Chem. Commun.*, 2013, **49**, 1471-1487.
8.　T. Kowada, H. Maeda and K. Kikuchi, *Chem. Soc. Rev.*, 2015, **44**, 4953-4972.
9.　L. Yuan, W. Lin, K. Zheng, L. He and W. Huang, *Chem. Soc. Rev.*, 2013, **42**, 622-661.
10.　D. Su, J. Oh, S.-C. Lee, J. M. Lim, S. Sahu, X. Yu, D. Kim and Y.-T. Chang, *Chem. Sci.*, 2014, **5**, 4812-4818.
11.　T. Papalia, G. Siracusano, I. Colao, A. Barattucci, M. C. Aversa, S. Serroni, G. Zappalà, S. Campagna, M. T. Sciortino, F. Puntoriero and P. Bonaccorsi, *Dyes Pigm.*, 2014, **110**, 67-71.
12.　T. Papalia, R. Lappano, A. Barattucci, A. Pisano, G. Bruno, M. F. Santolla, S. Campagna, P. De Marco, F. Puntoriero, E. M. De Francesco, C. Rosano, M. Maggiolini and P. Bonaccorsi, *Org. Biomol. Chem.*, 2015, **13**, 10437-10441.
13.　A. Kamkaew, S. H. Lim, H. B. Lee, L. V. Kiew, L. Y. Chung and K. Burgess, *Chem. Soc. Rev.*, 2013, **42**, 77-88.
14.　C. Zhang, J. Zhao, S. Wu, Z. Wang, W. Wu, J. Ma, S. Guo and L. Huang, *J. Am. Chem. Soc.*, 2013, **135**, 10566-10578.
15.　Y. Yang, Q. Guo, H. Chen, Z. Zhou, Z. Guo and Z. Shen, *Chem. Commun.*, 2013, **49**, 3940-3942.
16.　S. Guo, L. Ma, J. Zhao, B. Kucukoz, A. Karatay, M. Hayvali, H. G. Yaglioglu and A. Elmali, *Chem. Sci.*, 2014, **5**, 489-500.
17.　X.-F. Zhang and X. Yang, *J. Phys. Chem. B*, 2013, **117**, 5533-5539.
18.　X.-F. Zhang and X. Yang, *J. Phys. Chem. B*, 2013, **117**, 9050-9055.
19.　W. Li, L. Li, H. Xiao, R. Qi, Y. Huang, Z. Xie, X. Jing and H. Zhang, *RSC Adv.*, 2013, **3**, 13417-13421.
20.　A. B. Nepomnyashchii and A. J. Bard, *Acc. Chem. Res.*, 2012, **45**, 1844-1853.
21.　D. Frath, J. Massue, G. Ulrich and R. Ziessel, *Angew. Chem., Int. Ed.*, 2014, **53**, 2290-2310.
22.　S. Debnath, S. Singh, A. Bedi, K. Krishnamoorthy and S. S. Zade, *J. Phys. Chem. C*, 2015, **119**, 15859-15867.
23.　R. Ziessel, G. Ulrich, A. Haefele and A. Harriman, *J. Am. Chem. Soc.*, 2013, **135**, 11330-11344.
24.　J. Iehl, J.-F. Nierengarten, A. Harriman, T. Bura and R. Ziessel, *J. Am. Chem. Soc.*, 2012, **134**, 988-998.
25.　R. Ziessel and A. Harriman, *Chem. Commun.*, 2011, **47**, 611-631.
26.　B. Zheng, R. P. Sabatini, W.-F. Fu, M.-S. Eum, W. W. Brennessel, L. Wang, D. W. McCamant and R. Eisenberg, *PNAS*, 2015, **112**, E3987-E3996.

27. L. Dura, J. Ahrens, M.-M. Pohl, S. Höfler, M. Bröring and T. Beweries, *Chem. Eur. J.*, 2015, **21**, 13549-13552.
28. A. M. Poe, A. M. Della Pelle, A. V. Subrahmanyam, W. White, G. Wantz and S. Thayumanavan, *Chem. Commun.*, 2014, **50**, 2913-2915.
29. Y. Kubo, D. Eguchi, A. Matsumoto, R. Nishiyabu, H. Yakushiji, K. Shigaki and M. Kaneko, *J. Mater. Chem. A*, 2014, **2**, 5204-5211.
30. S. Kolemen, O. A. Bozdemir, Y. Cakmak, G. Barin, S. Erten-Ela, M. Marszalek, J.-H. Yum, S. M. Zakeeruddin, M. K. Nazeeruddin, M. Grätzel and E. U. Akkaya, *Chem. Sci.*, 2011, **2**, 949-954.
31. S. P. Singh and T. Gayathri, *Eur. J. Org. Chem.*, 2014, **2014**, 4689-4707.
32. V. Lakshmi, M. Rajeswara Rao and M. Ravikanth, *Org. Biomol. Chem.*, 2015, **13**, 2501-2517.
33. T. E. Wood and A. Thompson, *Chem. Rev.*, 2007, **107**, 1831-1861.
34. M. Cibian, A. Bessette, A. O'Connor, J. G. Ferreira and G. S. Hanan, *Acta Crystallogr., Sect. C*, 2015, **71**, 122-127.
35. A. Bessette, J. G. Ferreira, M. Giguère, F. Bélanger, D. Désilets and G. S. Hanan, *Inorg. Chem.*, 2012, **51**, 12132-12141.
36. Y. V. Zatsikha, E. Maligaspe, A. A. Purchel, N. O. Didukh, Y. Wang, Y. P. Kovtun, D. A. Blank and V. N. Nemykin, *Inorg. Chem.*, 2015, **54**, 7915-7928.
37. I. García-Moreno, L. Wang, A. Costela, J. Bañuelos, I. López Arbeloa and Y. Xiao, *ChemPhysChem*, 2012, **13**, 3923-3931.
38. L. Jiao, C. Yu, M. Liu, Y. Wu, K. Cong, T. Meng, Y. Wang and E. Hao, *J. Org. Chem.*, 2010, **75**, 6035-6038.
39. A. Bessette, M. Cibian, F. Belanger, D. Desilets and G. S. Hanan, *Phys. Chem. Chem. Phys.*, 2014, **16**, 22207-22221.
40. H. Liu, H. Lu, Z. Zhou, S. Shimizu, Z. Li, N. Kobayashi and Z. Shen, *Chem. Commun.*, 2015, **51**, 1713-1716.
41. S. Shimizu , A. Murayama, T. Haruyama, T. Iino, S. Mori, H. Furuta and N. Kobayashi *Chem. Eur. J.*, 2015, **21**, 12996-13003.
42. A. Wakamiya, T. Murakami and S. Yamaguchi, *Chem. Sci.*, 2013, **4**, 1002-1007.
43. E. Rousset, D. Chartrand, I. Ciofini, V. Marvaud and G. S. Hanan, *Chem. Commun.*, 2015, **51**, 9261-9264.
44. M.-P. Santoni, A. K. Pal, G. S. Hanan, M.-C. Tang, A. Furtos and B. Hasenknopf, *Dalton Trans.*, 2014, **43**, 6990-6993.
45. A. K. Pal, S. Serroni, N. Zaccheroni, S. Campagna and G. S. Hanan, *Chem. Sci.*, 2014, **5**, 4800-4811.
46. A. K. Pal, N. Zaccheroni, S. Campagna and G. S. Hanan, *Chem. Commun.*, 2014, **50**, 6846-6849.
47. A. K. Pal and G. S. Hanan, *Chem. Soc. Rev.*, 2014, **43**, 6184-6197.
48. Y. Ni, W. Zeng, K.-W. Huang and J. Wu, *Chem. Commun.*, 2013, **49**, 1217-1219.
49. Y. Ni and J. Wu, *Org. Biomol. Chem.*, 2014, **12**, 3774-3791.
50. M. Verdoes, U. Hillaert, B. I. Florea, M. Sae-Heng, M. D. P. Risseeuw, D. V. Filippov, G. A. van der Marel and H. S. Overkleeft, *Bioorg. Med. Chem. Lett.*, 2007, **17**, 6169-6171.
51. R. D. Rieth, N. P. Mankad, E. Calimano and J. P. Sadighi, *Org. Lett.*, 2004, **6**, 3981-3983.

52.   W.-C. Gao, S. Jiang, R.-L. Wang and C. Zhang, *Chem. Commun.*, 2013, **49**, 4890-4892.

53.   G. R. Humphrey and J. T. Kuethe, *Chem. Rev.*, 2006, **106**, 2875-2911.

54.   N. Kaewchangwat, R. Sukato, V. Vchirawongkwin, T. Vilaivan, M. Sukwattanasinitt and S. Wacharasindhu, *Green Chemistry*, 2015, **17**, 460-465.

55.   Preparation of para-nitro-phenyl substituted electron-poor BbF was not attainable in our hands using the described synthetic methodology.

56.   Y. Li, *Acc. Chem. Res.*, 2012, **45**, 723–733.

57.   N. Boens, V. Leen and W. Dehaen, *Chem. Soc. Rev.*, 2012, **41**, 1130-1172.

58.   N. Blouin, A. Michaud, D. Gendron, S. Wakim, E. Blair, R. Neagu-Plesu, M. Belletête, G. Durocher, Y. Tao and M. Leclerc, *J. Am. Chem. Soc.*, 2008, **130**, 732-742.

59.   V. Lakshmi, M. Shaikh and M. Ravikanth, *J. Fluoresc.*, 2013, **23**, 519-525.

60.   V. J. Richards, A. L. Gower, J. E. H. B. Smith, E. S. Davies, D. Lahaye, A. G. Slater, W. Lewis, A. J. Blake, N. R. Champness and D. L. Kays, *Chem. Commun.*, 2012, **48**, 1751-1753.

61.   Y. Tomimori, T. Okujima, T. Yano, S. Mori, N. Ono, H. Yamada and H. Uno, *Tetrahedron*, 2011, **67**, 3187-3193.

62.   C. Hansch, A. Leo and R. W. Taft, *Chem. Rev.*, 1991, **91**, 165-195.

63.   H. Svith, H. Jensen, J. Almstedt, P. Andersson, T. Lundbäck, K. Daasbjerg and M. Jonsson, *J. Phys. Chem. A*, 2004, **108**, 4805-4811.

64.   While the ground state electrochemistry of isolated molecules does not provide the formal EOx*, adding the ΔEOpt to the HOMO level provide a good first approximation based on the Rehm-Weller equation with no added work function term.

65.   Various values are reported in literature regarding the exact LUMO level of the PCBM vs vacuum. The value of -3.91 eV is from: He et al., Phys. Chem. Chem. Phys., 2011, 13, 1970-1983. The value of -4.3 eV is from: Blouin et al., J. Am. Chem. Soc. 2008, 130, 732-742.

66.   A. Hagfeldt, G. Boschloo, L. Sun, L. Kloo and H. Pettersson, *Chem. Rev.*, 2010, **110**, 6595-6663.

67.   S. M. McAfee, J. M. Topple, I. G. Hill and G. C. Welch, *J. Mater. Chem. A*, 2015, **3**, 16393-16408.

68.   K. Cnops, G. Zango, J. Genoe, P. Heremans, M. V. Martinez-Diaz, T. Torres and D. Cheyns, *J. Am. Chem. Soc.*, 2015, **137**, 8991-8997.

69.   D. Sun, D. Meng, Y. Cai, B. Fan, Y. Li, W. Jiang, L. Huo, Y. Sun and Z. Wang, *J. Am. Chem. Soc.*, 2015, **137**, 11156-11162.

70.   W. Senevirathna, J.-y. Liao, Z. Mao, J. Gu, M. Porter, C. Wang, R. Fernando and G. Sauve, *J. Mater. Chem. A*, 2015, **3**, 4203-4214.

71.   J. Zhao, Y. Li, H. Lin, Y. Liu, K. Jiang, C. Mu, T. Ma, J. Y. Lin Lai, H. Hu, D. Yu and H. Yan, *Energy Environ. Sci.*, 2015, **8**, 520-525.

72.   Y. Lin and X. Zhan, *Materials Horizons*, 2014, **1**, 470-488.

73.   K. Cnops, B. P. Rand, D. Cheyns, B. Verreet, M. A. Empl and P. Heremans, *Nat. Commun.*, 2014, **5**, 3406.

74.   P. Sonar, J. P. Fong Lim and K. L. Chan, *Energy Environ. Sci.*, 2011, **4**, 1558-1574.

75. M. C. Scharber, D. Mühlbacher, M. Koppe, P. Denk, C. Waldauf, A. J. Heeger and C. J. Brabec, *Adv. Mater.*, 2006, **18**, 789-794.
76. C. Yu, L. Jiao, H. Yin, J. Zhou, W. Pang, Y. Wu, Z. Wang, G. Yang and E. Hao, *Eur. J. Org. Chem.*, 2011, **2011**, 5460-5468.
77. L. Wang, Y. Zhang and Y. Xiao, *RSC Adv.*, 2013, **3**, 2203-2206.
78. B. Verbelen, S. Boodts, J. Hofkens, N. Boens and W. Dehaen, *Angew. Chem., Int. Ed.*, 2015, **54**, 4612-4616.
79. L. Wang, B. Verbelen, C. Tonnele, D. Beljonne, R. Lazzaroni, V. Leen, W. Dehaen and N. Boens, *Photochem. Photobiol. Sci.*, 2013, **12**, 835-847.
80. C. Yu, Y. Xu, L. Jiao, J. Zhou, Z. Wang and E. Hao, *Chem. Eur. J.*, 2012, **18**, 6437-6442.
81. K. Umezawa, A. Matsui, Y. Nakamura, D. Citterio and K. Suzuki, *Chem. Eur. J.*, 2009, **15**, 1096-1106.
82. A. Y. Bochkov, I. O. Akchurin, O. A. Dyachenko and V. F. Traven, *Chem. Commun.*, 2013, **49**, 11653-11655.
83. Y. V. Zatsikha, V. P. Yakubovskyi, M. P. Shandura, I. Y. Dubey and Y. P. Kovtun, *Tetrahedron*, 2013, **69**, 2233-2238.
84. C. Maeda, T. Todaka and T. Ema, *Org. Lett.*, 2015, **17**, 3090-3093.
85. K. Umezawa, Y. Nakamura, H. Makino, D. Citterio and K. Suzuki, *J. Am. Chem. Soc.*, 2008, **130**, 1550-1551.
86. K. Guzow, K. Kornowska and W. Wiczk, *Tetrahedron Lett.*, 2009, **50**, 2908-2910.
87. H. L. Kee, C. Kirmaier, L. Yu, P. Thamyongkit, W. J. Youngblood, M. E. Calder, L. Ramos, B. C. Noll, D. F. Bocian, W. R. Scheidt, R. R. Birge, J. S. Lindsey and D. Holten, *J. Phys. Chem. B*, 2005, **109**, 20433-20443.
88. P. Geerlings, S. Fias, Z. Boisdenghien and F. De Proft, *Chem. Soc. Rev.*, 2014, **43**, 4989-5008.
89. C. Adamo and D. Jacquemin, *Chem. Soc. Rev.*, 2013, **42**, 845-856.
90. D. Jacquemin, E. A. Perpète, I. Ciofini and C. Adamo, *Acc. Chem. Res.*, 2009, **42**, 326-334.
91. B. Le Guennic and D. Jacquemin, *Acc. Chem. Res.*, 2015, **48**, 530-537.
92. S. Chibani, B. Le Guennic, A. Charaf-Eddin, A. D. Laurent and D. Jacquemin, *Chem. Sci.*, 2013, **4**, 1950-1963.
93. D. Jacquemin, A. Planchat, C. Adamo and B. Mennucci, *J. Chem. Theo. Comp.*, 2012, **8**, 2359-2372.
94. S. Chibani, A. D. Laurent, B. Le Guennic and D. Jacquemin, *J. Chem. Theo. Comp.*, 2014, **10**, 4574-4582.
95. B. Le Guennic, O. Maury and D. Jacquemin, *Phys. Chem. Chem. Phys.*, 2012, **14**, 157-164.
96. Y. Chen, J. Zhao, H. Guo and L. Xie, *J. Org. Chem.*, 2012, **77**, 2192-2206.
97. S. Mukherjee and P. Thilagar, *RSC Adv.*, 2015, **5**, 2706-2714.
98. L. Zhang, L.-Y. Zou, J.-F. Guo, D. Wang and A.-M. Ren, *New J. Chem.*, 2015, ASAP.
99. R. L. Martin, *The Journal of Chemical Physics*, 2003, **118**, 4775-4777.
100. G. R. Desiraju and T. Steiner, *The Weak Hydrogen Bond: In Structural Chemistry and Biology*, Oxford University Press, New York, 2001.

101.   T. Dahl, *Acta Crystallogr., Sect. C*, 1985, **41**, 931-933.